17 July 1998

ELSEVIER

Chemical Physics Letters 291 (1998) 333–340

CHEMICAL PHYSICS LETTERS

# Mode specificity of vibrational energy relaxation of azulene in $CO_2$ at low and high density

C. Heidelbach, J. Schroeder *, D. Schwarzer, V.S. Vikhrenko [1]

*Max-Planck-Institut für Biophysikalische Chemie, D-37018 Göttingen, Germany*

Received 2 February 1998; in final form 12 May 1998

**Abstract**

Results of the normal mode analysis of classical molecular dynamics simulations of azulene vibrational energy relaxation in carbon dioxide are presented for the first time. There is strong evidence for different energy transfer mechanisms dominating at low and high densities. At low pressure only the low-frequency vibrational modes of the solute participate in the energy transfer to the solvent whereas at high pressure almost all the vibrational modes contribute to the solute-to-solvent energy flow. The relevance of these results for experimental studies is discussed. 

## 1. Introduction

In recent years systematic experimental investigations of vibrational energy relaxation (VER) of excited moderate size molecules in a variety of polyatomic solvents covering a broad range of solvent densities from gas to liquid phase have been performed [1–5]. The experimental data permitted to check the applicability of the isolated binary collision model (IBC) for the description of collisional energy transfer in the systems considered. Experimental investigations and their analysis in terms of IBC models only offer a restricted view of the dynamics of the processes operating on a molecular level, especially under high-density conditions which may, however, be studied in detail by computer simulations. As long as quantum dynamics computer simulations are feasible only for very simple systems classical molecular dynamics (MD) simulations (even if they do not correctly take into account the quantum mechanical nature of the high-frequency solute vibrational modes) can provide useful information for the understanding of vibrational energy transfer processes on a molecular level. The results of these calculations may create the basis for simpler model descriptions including quasiclassical and quantum dynamics considerations.

Numerous classical trajectory computations of collisional energy transfer have been done (see Refs. [6–8] and references therein) for low-pressure conditions. Using correlations between the distribution of vibrational frequencies of a solute and the rate of the vibrational energy transfer it was suggested [6] that the efficiency of energy transfer is enhanced by the presence of low-frequency vibrational modes. This suggestion is in agreement with theoretical models

* Corresponding author. E-mail: jschroe2@gwdg.de

[1] On leave from Belarussian State Technological University, Sverdlova Str. 13a, 220 630 Minsk, Belarus.

0009-2614/98/$19.00 
PII: S0009-2614(98)00589-2

describing individual oscillator vibrational relaxation which show that the efficiency of VER decreases exponentially with increasing oscillator frequency [9,10]. In this context the effect of the frequency spectrum of a moderate size solute on its vibrational relaxation in compressed gases and liquids is a question of great importance. In the present article we investigate the influence of solvent density on the collisional energy transfer mechanism. This is done by calculating the energy flux from individual vibrational modes of a highly excited polyatomic solute to the solvent.

## 2. Description of the model and MD procedure

The model used and the MD procedure carried out are described in detail elsewhere [11] and we only sketch their main characteristics. Classical microcanonical NEV molecular dynamics simulations have been performed [12] treating both solute and solvent completely flexible. The model system consists of one azulene ($C_{10}H_8$) molecule and 216 or 337 $CO_2$ molecules for low ($\approx 3.2$ MPa, $T \cong 445$ K, $\rho \cong 0.93$ mol/l) or high ($\approx 270$ MPa, $T \cong 298$ K, $\rho \cong 28{,}7$ mol/l) pressure simulations, respectively. $T$ and $\rho$ are the equilibrium solvent temperature and density at the beginning of the simulation. For both simulations the initial solute temperature was adjusted to 1100 K. The time step of integration was chosen as 0.5 fs. Short-range interactions were truncated at half the MD box length, whereas long-range electrostatic forces were treated with the Ewald summation technique [12]. All simulations were performed with the CHARMM [13] package which was modified to current needs. The simulations lasted 33 and 263 ps for high- and low-pressure conditions, respectively, because of the difference in cooling rates. We generated 40 trajectories for high pressure and 20 for low pressure to calculate the required averages; the numbers being limited by the total length of the simulations.

In our simulations we used the potentials of the model *b* as described in Ref. [11]. The $CO_2$ intramolecular potential was chosen in the form that takes into account stretch, bend and stretch–stretch harmonic interactions [14]. The azulene potential includes harmonic contributions from stretches, bends, improper torsions, and a cosine dependence on dihedral angles. Its parameters were tuned to reproduce experimental vibrational frequencies. The assignment of frequencies, their prescription to different types of vibrations and comparison with the experimental data [15] are presented in Table 1.

Though the individual 27 intramolecular bond stretch and bend potentials used are harmonic, they are kinematically coupled such that efficient intramolecular vibrational energy redistribution (IVR) may occur [16].

An exponential $-r^{-6}$ form with a coulomb term for atomic charge interaction [17] and state-dependent parameters tuned to reproduce experimental thermodynamic characteristics and neutron scattering data was adopted for the $CO_2$ intermolecular potential [18]. The azulene–$CO_2$ interaction was modelled by a combination of 6–12 potentials and coulomb interactions with pressure-independent parameters taken from the QUANTA database [19].

## 3. Theoretical background

The time derivative of the solute intramolecular, rotational and translational energy is equal to the capacity of external forces

$$\frac{\mathrm{d}E_1}{\mathrm{d}t} = \sum_{i=1}^{n} \mathbf{v}_i \cdot \mathbf{F}_i^{(\mathrm{e})}, \tag{1}$$

where $\mathbf{F}_i^{(\mathrm{e})}$ is the force exerted by all solvent atoms on nucleus $i$ of the solute, $\mathbf{v}_i$ is the velocity of nucleus $i$, and the summation is over all $n$ solute nuclei.

The solute energy $E_1$ can be divided into translational, rotational and internal vibrational energy. Such a division is not exact and we used Eckart's frame [16,20] to separate off the rotational and vibrational kinetic energy. Our simulation results have shown that the mean rotational and translational solute kinetic energy relax to solvent temperature on a subpicosecond timescale. The subsequent deactivation of the solute vibrational energy-by-energy transfer to the solvent is not affected substantially by the vibration–rotation interaction within the solute [21]. Hence the solute vibrational energy $E_{1\mathrm{vibr}}$ directly passes to the solvent through interactions between azulene vi-

Table 1
Calculated azulene normal mode frequencies and their symmetry

| Mode numbers | Frequencies ($cm^{-1}$) | | Symmetry |
|---|---|---|---|
| | Calc. | Exp. | |
| 1 | 185 | 189 | opa |
| 2 | 238 | 240 | ops |
| 3 | 327 | 304 | ops |
| 4 | 330 | 323 | ipa |
| 5 | 392 | 331 | opa |
| 6 | 395 | 406 | ips |
| 7 | 434 | 486 | ipa |
| 8 | 545 | 562 | ops |
| 9 | 554 | 542 | opa |
| 10 | 582 | 680 | ips |
| 11 | 588 | 731 | ops |
| 12 | 745 | 825 | ips |
| 13 | 759 | 712 | ipa |
| 14 | 785 | 900 | ips |
| 15 | 789 | 762 | ops |
| 16 | 852 | 813 | opa |
| 17 | 859 | 795 | ops |
| 18 | 866 | 987 | ipa |
| 19 | 916 | 952 | ops |
| 20 | 948 | 911 | opa |
| 21 | 967 | 965 | ops |
| 22 | 967 | 971 | ips |
| 23 | 999 | 941 | opa |
| 24 | 1016 | 1160 | ips |
| 25 | 1027 | 1058 | ops |
| 26 | 1029 | 1210 | ips |
| 27 | 1041 | 1012 | ipa |
| 28 | 1067 | 1049 | ipa |
| 29 | 1130 | 1117 | ipa |
| 30 | 1174 | 1268 | ips |
| 31 | 1224 | 1216 | ipa |
| 32 | 1296 | 1300 | ipa |
| 33 | 1398 | 1396 | ips |
| 34 | 1420 | 1378 | ipa |
| 35 | 1480 | 1443 | ipa |
| 36 | 1496 | 1448 | ips |
| 37 | 1528 | 1480 | ipa |
| 38 | 1578 | 1457 | ips |
| 39 | 1598 | 1579 | ips |
| 40 | 1642 | 1536 | ipa |
| 41 | 3028 | 2968 | ips |
| 42 | 3028 | 3018 | ipa |
| 43 | 3031 | 3037 | ips |
| 44 | 3034 | 3042 | ipa |
| 45 | 3036 | 3037 | ips |
| 46 | 3036 | 3077 | ipa |
| 47 | 3036 | 3072 | ips |
| 48 | 3039 | 3098 | ips |

In-plane symmetric (ips), in-plane asymmetric (ipa), out-of-plane symmetric (ops), out-of-plane asymmetric (opa).
Experimental values are identified by comparing frequencies and symmetries.

brational modes and the solvent molecules. If the vibration–rotation interaction is not taken into account the time derivative of $E_{1\mathrm{vibr}}$ is defined by an expression identical to Eq. (1) with the difference that total nuclear velocities $\mathbf{v}_i$ have to be replaced by vibrational velocities $\mathbf{u}_i$ of the nuclei which are defined by

$$\mathbf{u}_i = \mathbf{v}_i - \mathbf{v}_\mathrm{C} - \omega \times \mathbf{r}_{i\mathrm{C}} \,. \tag{2}$$

Here $\mathbf{v}_\mathrm{C}$ is the azulene centre-of-mass velocity, $\omega$ is the Eckart's frame rotational velocity and $\mathbf{r}_{i\mathrm{C}}$ is the position vector of the $i$th nucleus in the centre-of-mass frame.

Application of the normal mode analysis to a non-linear system is to some extent an artificial procedure. Nevertheless, it provides additional insight into processes that are collective or many-body in origin. Even for such strongly non-linear systems as liquids the instantaneous normal mode analysis yields essential information [22,23] about their static and dynamic properties including solvation and relaxation processes. The normal modes being originally introduced in a linear approximation reproduce some characteristics of non-linear systems exactly, e.g. those which are of quadratic (such as kinetic energy) or bilinear form.

From the normal mode analysis of the isolated azulene molecule we derived the orthonormalized transition matrix $\mathbf{P}_{\alpha i}$. Subsequently, normal mode velocities $\dot{q}_\alpha$ and external normal forces $Q_\alpha^{(\mathrm{e})}$ can be introduced

$$\dot{q}_\alpha = \sum_{i=1}^{n} \mathbf{P}_{\alpha i}^{t} \cdot \sqrt{m_i}\, \mathbf{u}_i, \qquad \alpha = 1, 2, \ldots, 3n-6, \tag{3}$$

$$Q_\alpha^{(\mathrm{e})} = \sum_{i=1}^{n} \mathbf{F}_i^{(\mathrm{e})} \cdot \frac{1}{\sqrt{m_i}} \mathbf{P}_{i\alpha} \,. \tag{4}$$

The rhs of Eq. (1) and of the corresponding equation for $E_{1\mathrm{vibr}}$ are bilinear in velocities and forces. Hence both can identically be represented by external normal forces and normal mode velocities such that the equation describing the evolution of the solute internal vibrational energy $E_{1\mathrm{vibr}}$ attains the form [21]

$$\frac{\mathrm{d}E_{1\mathrm{vibr}}}{\mathrm{d}t} = \sum_{\alpha=1}^{3n-6} \dot{q}_\alpha \cdot Q_\alpha^{(\mathrm{e})} \,. \tag{5}$$

Due to anharmonicities the solute vibrational energy has to be represented as a sum of normal mode energies and terms which describe non-linear interactions. Therefore, the equations of motion for normal co-ordinates include [21] the external normal forces and, in addition, internal intermode non-linear coupling terms $Q_\alpha^{(\mathrm{i})}$

$$\frac{\mathrm{d}\dot{q}_\alpha}{\mathrm{d}t} + \omega_\alpha^2 q_\alpha = Q_\alpha^{(\mathrm{e})} + Q_\alpha^{(\mathrm{i})}\,, \tag{6}$$

where $\omega_\alpha^2$ is the squared $\alpha$th normal mode frequency.

The $Q_\alpha^{(\mathrm{i})}$ in Eq. (6) govern the intramolecular and vibrational-to-rotational redistribution of energy while the $Q_\alpha^{(\mathrm{e})}$ describe the interactions of the $i$th vibrational mode with the solvent. Hence capacities $Q_\alpha^{(\mathrm{i})} \cdot \dot{q}_\alpha$ and $Q_\alpha^{(\mathrm{e})} \cdot \dot{q}_\alpha$ can be regarded as the energy exchange rates between a particular solute mode $\alpha$ and the remainder of the solute and the solvent, respectively. The total energy transferred via the $\alpha$th normal mode to the solvent in time $t$ is defined by the integral of the capacity

$$W_\alpha = -\int_0^t \dot{q}_\alpha Q_\alpha^{(e)} \mathrm{d}t\,. \tag{7}$$

The distribution of $W_\alpha$ over $\alpha$ represents the contribution of each particular solute normal mode to the solute–solvent energy exchange.

## 4. Simulation results and discussion

The simulated VER of the solute potential and kinetic energy was shown to be monoexponential in time at low and high pressure with relaxation times of 306 and 12.5 ps, respectively [11]. These results reasonably agree with the trend seen in experimental values of 213 and 18.7 ps, respectively [3]. Among the possible reasons behind the discrepancy between simulated and experimental cooling rates, the most important probably is that the azulene–$CO_2$ interaction potential from the QUANTA database was used without tuning its parameters to reproduce characteristics of the real system such as translational and

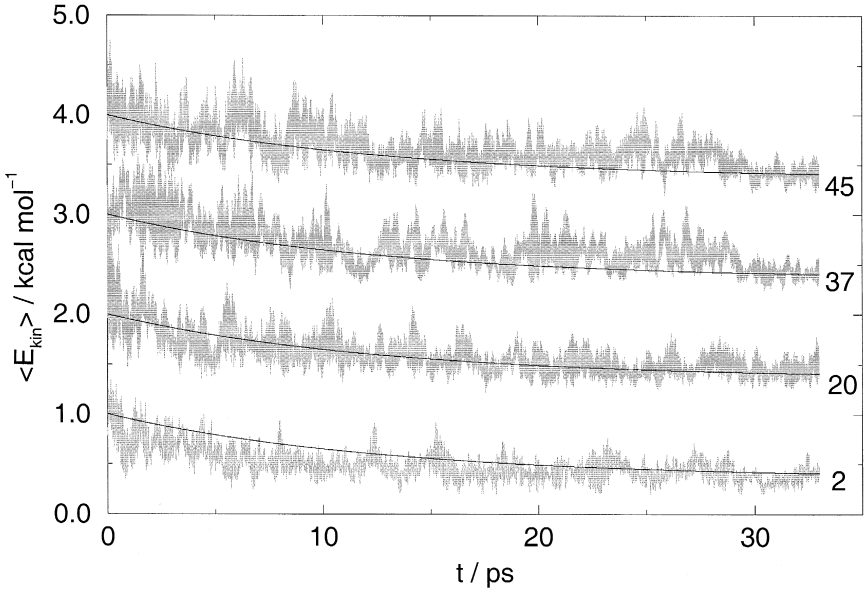


Fig. 1. Kinetic vibrational energies versus time for selected azulene normal modes during the energy relaxation (frequencies and symmetry of normal modes: $\omega_2 = 238$ cm$^{-1}$, out-of-plane symmetric (ops); $\omega_{20} = 948$ cm$^{-1}$, out-of-plane asymmetric (opa); $\omega_{37} = 1528$ cm$^{-1}$, in-plane asymmetric (ipa); $\omega_{45} = 3037$ cm$^{-1}$, in-plane symmetric (ips)) at high-pressure conditions. Each curve is shifted upward by 1 kcal/mol with respect to previous one. The smooth curves represent the total energy decay and just meant to guide the eye.

rotational diffusion coefficients or the partial molar volume in the limit of small azulene concentration. Another reason may be that the intramolecular azulene potential was tuned only to experimental vibrational frequencies without considering anharmonicities of the intramolecular modes. However, the potential led to fast IVR rates in the simulations indicating that these deficits may be not essential. A more serious problem could be the classical treatment of high-frequency solute vibrational modes.

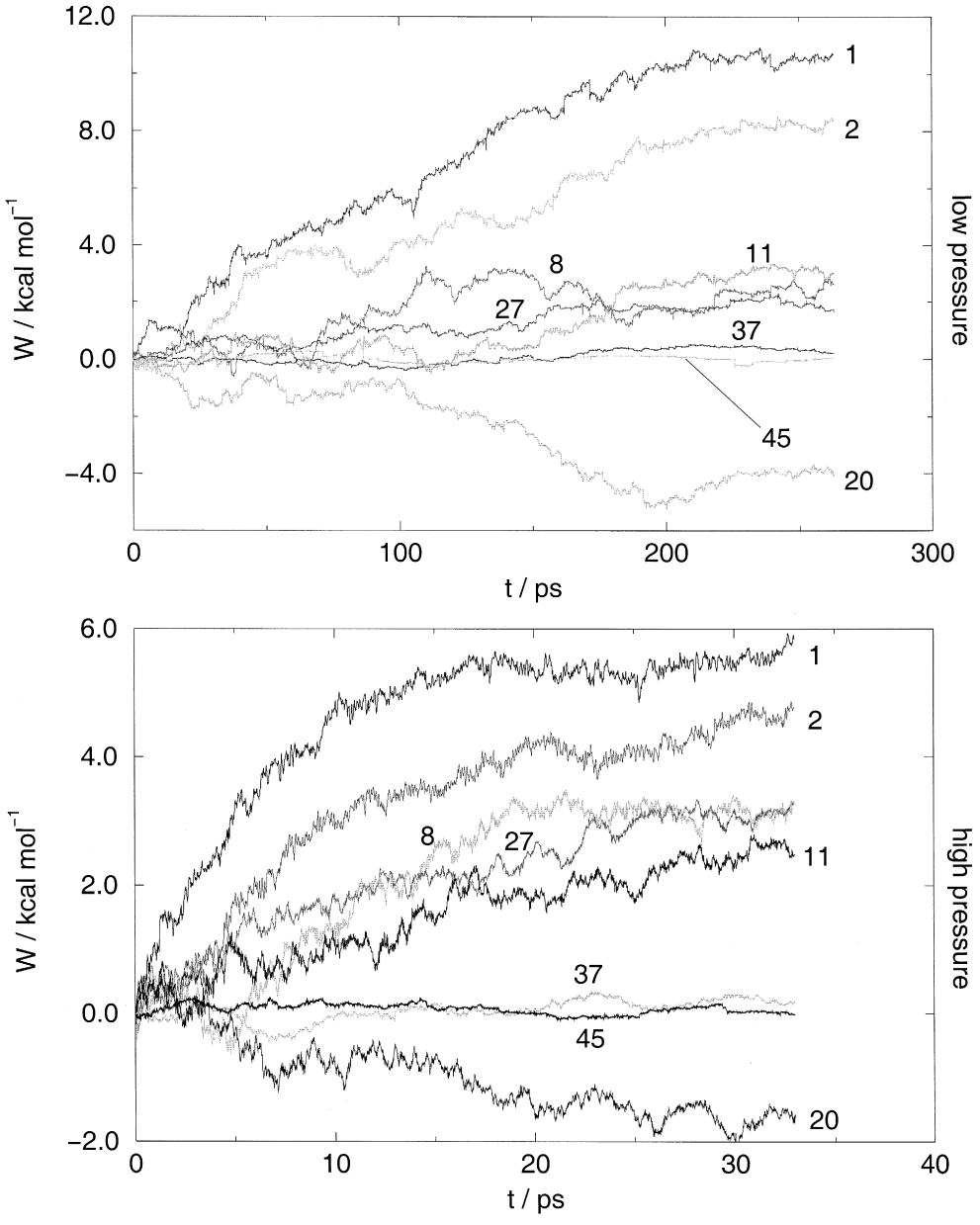


Fig. 2. The energy transferred by particular modes (curves are lettered by mode numbers) versus time (frequencies and symmetry of normal modes: $\omega_1 = 186$ cm$^{-1}$, opa; $\omega_2 = 238$ cm$^{-1}$, ops; $\omega_8 = 546$ cm$^{-1}$, ops; $\omega_{11} = 588$ cm$^{-1}$, ops; $\omega_{20} = 948$ cm$^{-1}$, opa; $\omega_{27} = 1042$ cm$^{-1}$, ipa; $\omega_{37} = 1528$ cm$^{-1}$, ipa; $\omega_{45} = 3037$ cm$^{-1}$, ips).

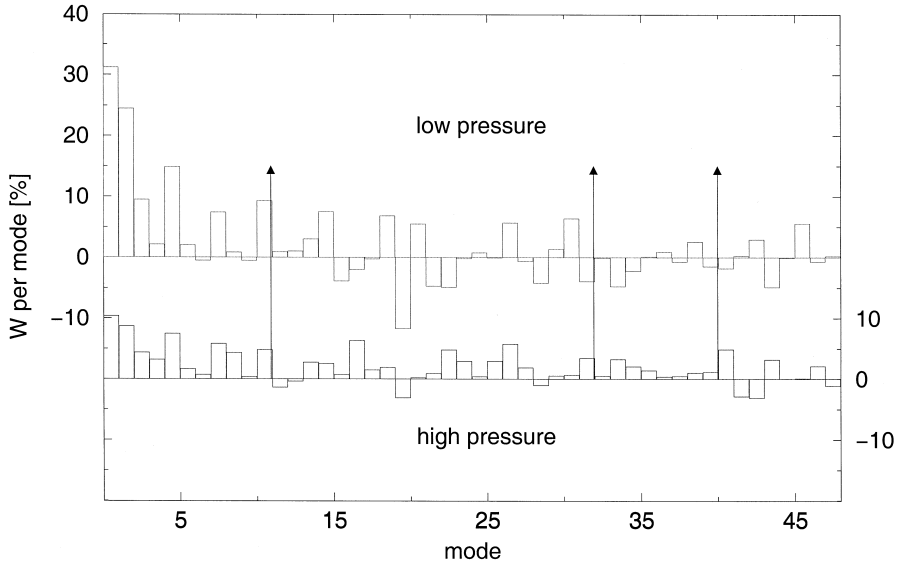


Fig. 3. The distribution of energy transferred by particular normal modes during the simulation time. The $CO_2$ normal frequencies [28] are indicated by arrows. The highest $CO_2$ frequency $\omega_4' = 2329\ cm^{-1}$ lies between the azulene frequencies $\omega_{40} = 1542\ cm^{-1}$ and $\omega_{41} = 3028\ cm^{-1}$.

Although there are many indications [24–27] that a classical description of VER can be quite satisfactory, this need not be the case in our simulations.

In Fig. 1 the time evolution of the kinetic energy for individual modes taken from different spectral regions is shown. It appears that for all normal modes the energy decays are on the same timescale. This indicates that our azulene potential ensures an effective intramolecular energy redistribution. In Fig. 2 the energy transferred by individual solute modes to the solvent as calculated by Eq. (7) is plotted versus time. Although the internal vibrational energy of the azulene molecule is well equilibrated at all times the contribution to the solute-to-solvent energy

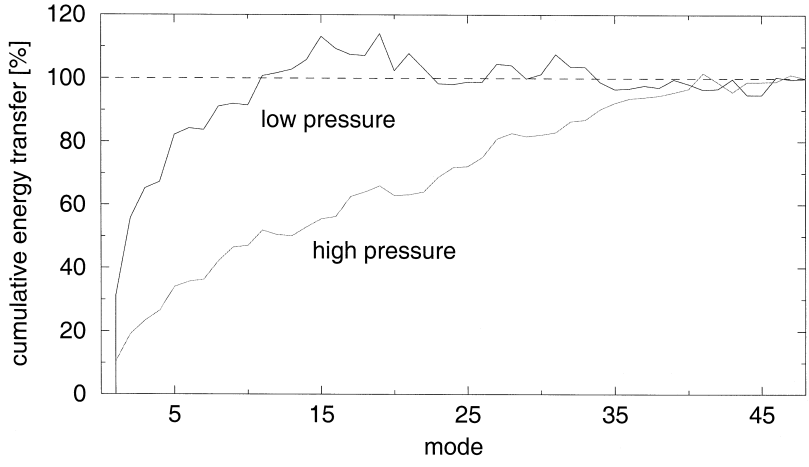


Fig. 4. The energy transferred by all the lowest modes up to the $n$th one versus $n$.

exchange differs drastically from one mode to another and strongly depends on thermodynamic conditions. Fig. 2 clearly shows that the lowest vibrational modes of 185 and 238 $cm^{-1}$ contribute most to the energy transfer both at low and at high density. However, the fraction of energy transferred to the solvent via these modes is a factor of about 3 higher at low pressure. It is interesting to note that some modes (e.g. $i = 20$) gain energy from the solvent. Some other modes are almost inactive ($i = 37, 45$) showing small fluctuations with negligible energy flow. Of course, these differences depend on the details of the collective motion connected with the specific structure of the azulene normal mode vector, geometric and force characteristics of the $CO_2$ molecules, and thermodynamic conditions which define the mutual azulene–$CO_2$ space distribution [11]. For $i = 20$ the mode structure is such that the direction of the solvent-to-solute energy flow remains stable over a two order of magnitude change in pressure. The same is true with respect to the inactivity of modes 37 and 45.

The distribution of energy transferred through particular modes is plotted versus mode number in Fig. 3. At low pressure 80% of the energy is dissipated via the five lowest frequency modes, a result in agreement with conclusions derived from classical trajectory calculations [6]. At high pressure this behaviour changes significantly; now the five lowest-frequency modes transfer only 30% of the energy. This qualitative change of the energy transfer mechanism is also visible in Fig. 2.

The contrasting behaviour of the low- and high-pressure energy flow data appear even more dramatic in Fig. 4, where the accumulation of the energy transfer by all modes $i \leqslant n$ is plotted versus $n$. At low pressure all the energy is transferred by approximately 11 low-frequency modes ($\omega_{11} = 588$ $cm^{-1}$) and the other modes take part in intramolecular energy redistribution accompanied by intermolecular collisions. At high pressure, modes up to $i = 40$ ($\omega_{40} = 1642$ $cm^{-1}$) take part in the intermolecular energy transfer. The relative contribution of high-frequency modes to the energy transfer moderately decreases as the frequency increases. However, a correlation with the $CO_2$ normal frequencies, denoted by arrows in Fig. 3, cannot be detected. The manifold of available channels for energy flow due to combination of different solute and solvent modes masks direct resonances between the azulene and $CO_2$ vibrational modes.

To explain such peculiarities one has to resort to Eq. (4) for the normal force. It says that the external force $\mathbf{F}_i^{(e)}$ acting on a single solute atom $i$ gives rise to many (or even all) normal forces $Q_\alpha^{(e)}$. The latter depend on the direction of the normal vectors forming the basis of the transition matrix $\mathbf{P}_{\alpha i}$. Hence during each single azulene–$CO_2$ collision intramolecular intermode energy exchange takes place which results in intramolecular vibrational energy redistribution. Moreover, during the collision $CO_2$ usually interacts with several azulene atoms.

At low pressure many of the high-frequency normal modes are active. However, their activity probably results in collisionally assisted IVR processes. The energy transfer distribution presented in Figs. 3 and 4 gives reason for such an assumption. The spectral diapason above 600 $cm^{-1}$ seems to be determined by elastic interactions between azulene and $CO_2$ molecules.

In contrast at high pressure the dense environment apparently has a dissipative effect on colliding partners and modes that transfer energy from the solvent to the solute almost do not exist. The spectral diapason of the C–H stretch vibrations ($\approx 3000$ $cm^{-1}$) is inactive and reflects the elastic character of intermolecular interactions at high pressure as well.

To support these assumptions the analysis of time correlation functions of the normal forces, normal mode velocities and energy flows will have to be done.

## 5. Conclusions

The normal mode analysis of MD simulation data reveals pronounced differences between solute–solvent energy exchange mechanisms at low and high solvent density. At low density the main contribution to the energy flow comes from the lowest vibrational modes. In the spectral diapason $\omega > 600$ $cm^{-1}$ collisionally assisted intramolecular energy redistribution takes place; solute–solvent interaction has an elastic character. At high-pressure normal modes from the whole spectral diapason except for H–C stretch vibrations are incorporated in VER

processes with moderately decreasing quota at higher frequencies. Still some particular modes remain inactive and do not contribute to the energy exchange.

No evidence for correlations between the solute mode activity and the $CO_2$ vibrational spectrum was found. Hence for understanding the role of solvent vibrations and the distribution of energy transferred into the accepting modes of the solvent additional simulations have to be done. The analysis of trajectory calculations could also benefit from the type of normal mode analysis we have presented here to shed light on peculiarities of energy transfer in purely binary collisions.

## Acknowledgements

The authors are grateful to the Volkswagen Stiftung for financial support of the collaboration project (I70/627).

## References

[1] T. Elsaesser, W. Kaiser, Annu. Rev. Phys. Chem. 42 (1991) 83.
[2] K. Lenz, M. Pfeifer, A. Lau, T. Elsaesser, Chem. Phys. Lett. 229 (1994) 340.
[3] D. Schwarzer, J. Troe, M. Votsmeier, M. Zerezke, J. Chem. Phys. 105 (1996) 3121.
[4] J. Benzler, S. Linkersdörfer, K. Luther, J. Chem. Phys. 106 (1997) 4992.
[5] D. Schwarzer, J. Troe, M. Zerezke, J. Chem. Phys. 107 (1997) 8380.
[6] T. Lenzer, K. Luther, J. Troe, R. Gilbert, K.F. Lim, J. Chem. Phys. 103 (1995) 626.
[7] R.G. Gilbert, Austr. J. Chem. 48 (1995) 1787.
[8] G. Lendvay, G.C. Schatz, Adv. Chem. Kin. Dyn. 28 (1995) 481.
[9] S.A. Adelman, R. Mularidhar, R.H. Stote, J. Chem. Phys. 95 (1991) 2738.
[10] S.A. Egorov, J.L. Skinner, J. Chem. Phys. 105 (1996) 7047.
[11] C. Heidelbach, I. Fedchenia, D. Schwarzer, J. Schroeder, J. Chem. Phys. 108 (1998) 10152.
[12] M.P. Allen, D.J. Tildesly, Computer Simulation of Liquids (Oxford University Press, Oxford, 1987).
[13] Harvard University. Charm 24.b1 (1995).
[14] S.-B. Zhu, G.W. Robinson, Comp. Phys. Commun. 52 (1989) 317.
[15] R.S. Chao, R.K. Khanna, Spectrochim. Acta 33A (1977) 53.
[16] E.B. Wilson Jr., J.C. Decius, P.C. Cross, Molecular Vibrations: The Theory of Infrared and Raman Vibrational Spectra (McGraw–Hill, New York, NY, 1955).
[17] H.J. Böhme, C. Meissner, R. Ahlrichs, Mol. Phys. 53 (1984) 672.
[18] I.I. Fedchenia, J. Schroeder, J. Chem. Phys. 106 (1997) 7749.
[19] Molecular Simulation. Quanta 4.0 (1994).
[20] C. Eckart, Phys. Rev. 47 (1935) 552.
[21] V.S. Vikhrenko, C. Heidelbach, V.B. Nemtsov, D. Schwarzer, J. Schroeder, manuscript in preparation.
[22] P. Moore, A. Tokmakoff, T. Keyes, M.D. Fayer, J. Chem. Phys. 103 (1995) 3325.
[23] G. Goodyear, R.M. Stratt, J. Chem. Phys. 107 (1997) 3098.
[24] M.A. Collins, H.S. Schranz, J. Chem. Phys. 100 (1994) 2089.
[25] H.S. Schranz, M.A. Collins, J. Chem. Phys. 101 (1994) 307.
[26] J.S. Bader, B.J. Berne, J. Chem. Phys. 100 (1994) 8359.
[27] S.A. Egorov, B.J. Berne, J. Chem. Phys. 107 (1997) 6050.
[28] S.-B. Zhu, G.W. Robinson, Comp. Phys. Commun. 52 (1989) 317.